The Effect of Dissolved Hydrogen on Fuel Crud and Oxide Layer of Fuel Clad in Sub-cooled Nucleate Boiling Condition of PWR Primary Water

Sieun Baek[a,b], Min-gyo Seo[a], Suyong Jo[a,b], Do Haeng Hur[a], Hyo-Sik Chang[b], Hee-Sang Shim[a,*]
[a]*Materials Safety Technology Research Division, KAERI, 989-111 Daedeok-daero, Yuseong-gu, Daejeon 34057, Korea*
[b]*Graduate School of Energy Science and Technology, Chungnam National University, Daejeon, 34134, Korea*
[*]*Corresponding author: hshim@kaeri.re.kr*

Keywords : Crud, Oxide Layer, Dissolved Hydrogen, Sub-Cooled Nucleate Boiling, PWR

1. Introduction

In the primary coolant system of pressurized water reactors (PWRs), various corrosion products are generated due to the corrosion of structural materials and fuel cladding tubes in a high-temperature, high-pressure water environment. These corrosion products migrate with the coolant and are deposited on the surface of nuclear fuel cladding tubes under subcooled nucleate boiling (SNB) condition. The deposited layer formed on the cladding surface is termed crud (Chalk River Unidentified Deposit or Corrosion-Related Unidentified Deposit), and crud is recognized as one of the primary factors threatening nuclear fuel integrity [1,2].

Crud typically exhibits a porous structure composed mainly of Ni–Fe oxides and shows low effective thermal conductivity. Consequently, when crud is deposited on the surface of fuel cladding tubes, local thermal resistance can increase, leading to elevated cladding surface temperatures. This temperature rise may accelerate oxidation reactions of the cladding, potentially affecting oxide growth behavior and hydrogen uptake [2,3]. Furthermore, the porous crud structure can induce localized changes in the chemical environment, such as the accumulation of dissolved ions and localized pH variations, which can further exacerbate the oxidation and corrosion behavior of the cladding beneath the crud layer. This phenomenon of accelerated local corrosion of fuel cladding due to crud is called crud-induced localized corrosion (CILC), and is an important factor in monitoring the integrity of nuclear fuel.

Corrosion rate of zirconium-based alloys has been reported to be influenced by various factors, including material properties, processability, water chemistry and thermal-hydraulic conditions, hydride fraction, and surface deposits [4,5]. However, zirconium-based alloys form a uniform internal oxide layer and exhibit low corrosion rates under PWR operating conditions, particularly within the 280~360°C temperature range. However, the corrosion rate of zirconium-based alloys increased rapidly as the temperature increased above 320°C, and its dependence on material properties, particularly chemical composition and microstructure, was also significant. Among water chemistry environmental factors, the dissolved hydrogen concentration in the reactor coolant has well known to significantly impact the structural integrity of zirconium-based alloys. Thermal neutrons generated during the chain fission reaction of nuclear fuel cause water to radioactively decompose, generating hydrogen. This hydrogen readily diffuses into the zirconium-based alloy cladding during the corrosion reaction, forming hydrides [6]. These hydrides, which are less ductile than the surrounding metal matrix, can have deleterious effects on the mechanical properties of these components when present at sufficiently high-volume fraction. Although the risk of hydride has reported to be minimal within dissolved hydrogen concentration range of the PWR normal operation condition, evaluating the effect of dissolved hydrogen concentration on zirconium-based alloy cladding is required because local water chemistry may change into a critical environment if crud deposited heavily on it.

Therefore, we compared the corrosion behaviors of Zr-1.0Nb-1.0Sn alloy with and without crud under simulated water chemistry conditions of PWR with different dissolve hydrogen concentrations in this work. In addition, the crud and zirconium oxide layer of oxidized and crud-deposited fuel claddings were analyzed for the specimens before and after the accelerated corrosion test.

2. Experimental method

The corrosion experiments in this study were conducted using a high-temperature, high-pressure water chemistry circulation loop simulating a PWR primary system (Fig. 1). The experiments were performed under subcooled nucleate boiling (SNB) conditions at 325 °C, 15 MPa, and $pH_{325°C}$ = 6.9. Zr–1.0Sn–1.0Nb alloy fuel cladding tube specimens with and without crud deposition were investigated. The dissolved hydrogen (DH) concentration was controlled at two levels corresponding to the operating range of commercial nuclear power plants, namely 25 and 50 cc/kg·H_2O.

The specimens were prepared by sealing both ends of the fuel cladding tubes, inserting cartridge heaters, and connecting them to the autoclave head to form the test section. For the accelerated corrosion tests, a 150 mm-long section was cut from the crud-deposited fuel cladding tube, whereas a 300 mm-long section was cut from the fuel cladding tube without crud deposition. These sections were connected using the fitting, inserted by a cartridge heater, and then fixed to the test section. The top-left schematic in Fig. 1 illustrates the simulated primary coolant loop for the corrosion of the fuel cladding tube and the top-right schematic shows the simulated primary coolant loop for the crud deposition

on the fuel cladding. In addition, the bottom schematic presents the simulated primary coolant loop for the accelerated corrosion test of the connected specimens.

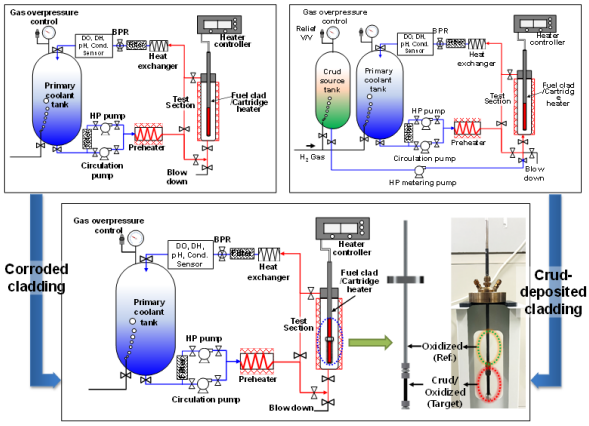

Fig. 1. Schematic diagram of the experimental loops in simulated primary coolant conditions for corrosion, crud deposition, and accelerated corrosion.

The simulated primary coolant was prepared with 1.08 ppm lithium (as LiOH) and 1,000 ppm boron (as H_3BO_3). The dissolved oxygen concentration was controlled below 5 ppb through injecting the hydrogen gas into the coolant tank. The DH concentration was controlled by 25 and 50 cc/kg·H_2O as the upper and lower limits of the operating range of the PWRs. Crud source solutions were prepared by dissolving Ni–EDTA (ethylenediamine-tetraacetic acid disodium nickel(II) hydrate) and iron acetate ($Fe(CO_2CH_3)_2$) in 50 L DI water at concentrations to be 1,500 ppm and 2,000 ppm, respectively.

Table 1. Chemical composition and mechanical properties of zirconium alloy cladding tube.

Test No.	Coolant		Crud source		pH 325℃	Temp (℃)	DH (cc/kg·H_2O)	P (MPa)	Test Time (h)
	Li conc. (ppm)	B conc. (ppm)	Ni conc. (ppm)	Fe conc. (ppm)					
1-1	1.08	1,000	-	-	6.9	325	35	15	250
1-2	1.08	1,000	1,500	2,000	6.9	325	35	15	250
2-1	1.08	1,000	-	-	6.9	325	25	15	500
2-2	1.08	1,000	-	-	6.9	325	50	15	500

Fuel cladding corrosion and crud deposition were carried out in DH condition of 35 cc/kg·H_2O for 250 h. After the first stage experiment was completed, the specimen for accelerated corrosion test was prepared by cutting the upper 400 mm of the corroded cladding and the lower 100 mm of the crud-deposited cladding, and by connecting with fitting unit. The accelerated corrosion test was performed for 500h in the same primary coolant condition as the corrosion experiment in step 1 with controlling DH to 25 and 50 cc/kg·H_2O. Detailed experimental conditions are summarized in Table 1. The structural and compositional characteristics of the crud before and after the corrosion tests were analyzed using FIB–SEM, SEM–EDS, and XRD.

3. Results and discussion

Fig. 2 shows the characteristics of the crud in the crud-deposited fuel cladding to compare the corrosion acceleration with the corroded fuel cladding. The surface of the crud shows extremely rough due to numerous pores and protrusions measuring several micrometers in size as shown in Fig. 2(a). In addition, the thickness of crud was observed differently according to the location in the range of 100~150 μm as shown in Fig. 2(b) and its porosity increased from the metallic cladding matrix toward the crud/coolant interface. Then, the average porosity is 29.6% and evaluated in the range of 19.4% ~42.8%. The chemical composition of crud shows the mixture of $(Ni+Fe)_2O_3$ and $(Ni+Fe)_3O_4$ and the (Ni+Fe)/O ratio is about 0.9 as shown in Fig. 2(c) and chemical composition table. Considering the inaccuracy of the analytical resolution of SEM-EDS, further analysis such as XRD or TEM-EDS is necessary to confirm accurately the chemical composition of crud.

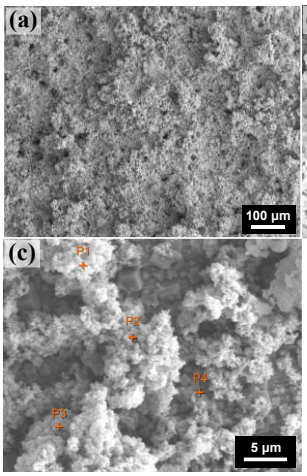

Site	Element (at%)			
	Ni	Fe	O	Total
P1	12.29	33.22	54.49	100
P2	13.70	34.08	52.22	100
P3	11.21	32.68	56.11	100
P4	10.93	41.32	47.75	100
Ave.	12.03	35.33	52.64	100

Fig. 2. SEM images and EDS analysis of the fuel cladding with crud deposition before corrosion testing: (a) surface SEM image of the crud-deposited cladding, (b) cross-sectional SEM image of the crud-deposited cladding, (c) EDS analysis results of the crud-deposited cladding.

The surface morphology of the fuel claddings corroded for 250h and for 750h was analyzed using SEM and EDS as shown in Fig. 3. Fig. 3(a) and 3(b) present the surface images of the fuel claddings which are corroded for 250h at DH concentrations of 25 cc/kg·H_2O and 50 cc/kg ·H_2O, respectively. Polishing marks were observed on the surfaces of both specimens before the accelerated corrosion test, and it was difficult to find differences between two specimens. However, it was found that numerous polyhedral particulate oxides were formed on the surfaces of both specimens after the accelerated corrosion tests. Fig. 3(e) and 3(d) are EDS point analysis results from Fig. 3(c) and 3(d), which show that in addition to the zirconium oxide layer, oxides including Ni and Fe were newly observed. These are believed to have been eroded, migrated and deposited from the oxidized specimen of the fuel cladding and the crud-deposited specimen connected by fitting.

The surface morphology of crud layers is similar to the specimen before the accelerated corrosion test as shown in Fig. 4(a) and 4(b), in which numerous pores and protrusions observed.

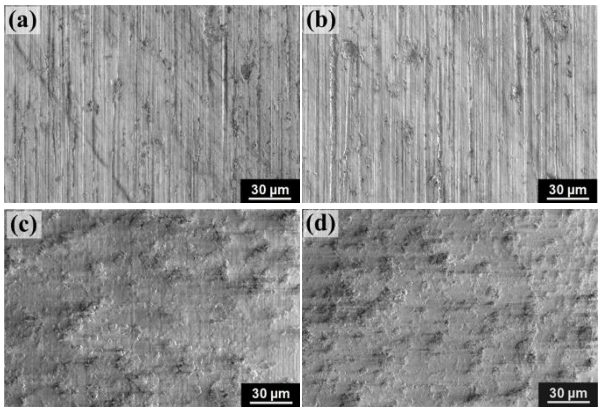

(e) Site	Element (at%)					
	Zr	O	Nb	Sn	Fe	Ni
P1	50.84	49.16	-	-	-	-
P2	51.81	48.19	-	-	-	-
P3	51.24	48.33	-	0.42	-	-
P4	29.91	56.85	1.44	0.26	9.50	2.03

(f) Site	Element (at%)					
	Zr	O	Nb	Sn	Fe	Ni
P1	54.58	45.02	-	0.40	-	-
P2	46.43	53.57	-	-	-	-
P3	48.78	50.85	-	0.37	-	-
P4	4.66	60.33	-	-	33.70	1.31

Fig. 3. SEM images of corroded fuel cladding before and after accelerated corrosion tests: (a) before test at DH 25 cc/kg·H_2O, (b) before test at DH 50 cc/kg·H_2O, (c) after test at DH 25 cc/kg·H_2O, (d) after test at DH 50 cc/kg·H_2O.

However, the cross-section of crud layer looks more denser than before the test, and few cracks are observed. This would be because the coalescence of oxide particles and erosion into the coolant simultaneously occurred under the continued SNB condition. In addition, it is believed that some of the eroded crud moved to and deposited to the surface of the corroded cladding specimen connected at the top. Due to this reason, the crud thickness is measured to have decreased by approximately 50% from 100~150 μm before the corrosion test to 60~80 μm.

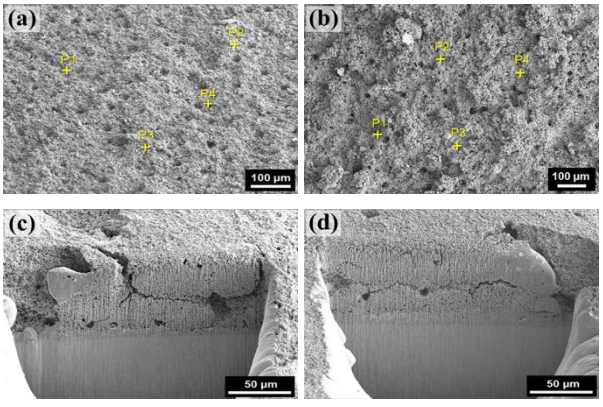

(e) Site	Element (at%)			
	Ni	Fe	Zr	O
P1	14.72	45.02	1.67	45.52
P2	16.51	53.57	4.20	59.96
P3	11.90	50.85	4.22	52.40
P4	18.31	60.33	3.73	49.61

(f) Site	Element (at%)			
	Ni	Fe	Zr	O
P1	16.89	41.48	0.86	40.77
P2	13.99	42.23	2.34	41.44
P3	14.97	40.14	1.45	43.44
P4	14.48	36.87	2.08	46.57

Fig. 2. SEM–EDS analysis results of the crud-deposited cladding after corrosion test for 500h: (a)(c) DH 25 cc/kg·H_2O, (c)(d) DH 50 cc/kg·H_2O.

The change in thickness of zirconium dioxide (ZrO_2) is negligible for each fuel cladding specimens with and without crud between DH concentrations as summarized in Table 2. While, the acceleration of cladding corrosion due to crud deposition was analyzed to be 7~9% greater under both dissolved hydrogen conditions. This tendency suggests that the presence of crud alters the local heat transfer conditions at the cladding surface. Due to the lower thermal conductivity of the crud layer compared to that of the zirconium alloy, additional thermal resistance can be introduced at the cladding surface, leading to a locally elevated temperature beneath the crud. While the change for the DH concentration was very small. Therefore, it can be judged that the DH concentration in the coolant system has no effect on the acceleration of cladding corrosion within the normal operating condition, and the effect due to crud deposit is that corrosion is accelerated by about 8% compared to general cladding corrosion.

Table 2. Average oxide thickness of fuel cladding with and without crud before and after corrosion tests under different DH conditions

DH (cc/kg·H_2O)	Type of specimen	ZrO_2 Ave. thickness (μm)		
		Before test	After test	Change (%)
25	Cladding	0.90	1.14	26.7
	Crud with	0.85	1.15	35.3
50	Cladding	0.92	1.17	27.2
	Crud with	0.87	1.18	35.6

4. Conclusions

In this study, a high-temperature, high-pressure water chemistry loop was used to simulate subcooled nucleate boiling conditions, and the effects of DH on the corroded fuel cladding and the crud-deposited fuel cladding were investigated in the point of change of crud layer and corrosion rate. The DH concentration was controlled at 25 and 50 cc/kg·H_2O. The results indicated that crud deposition significantly modifies the corrosion behavior of zirconium alloy cladding by altering local thermal and chemical condition but the DH concentration is negligible to the corrosion of fuel cladding in the PWR normal operation conditions. In addition, much amount of crud is eroded into the coolant, migrated and deposited other location. These findings provide insight into the combined influence of crud and DH on cladding corrosion and contribute to understanding corrosion mechanism relevant to CILC under PWR operating conditions.

Acknowledgments

This work was financially supported by the Korea Institute of Energy Technology Evaluation and Planning (KETEP) grant (RS-2025-02311389) and the National Research Foundation (NRF) grant (RS-2022-00143316) funded by the Korea government.

REFERENCES

[1] H. He, Y. Liu, S. Wang, et al., Review on corrosion-related unidentified deposit of pressurized water reactors, Nuclear Engineering and Design, Vol. 441, 114095, 2025.
[2] C. Xue, Y. Mao, Z. Zhang, et al., Crud deposition behavior on zirconium alloy fuel cladding in high-temperature pressurized water environments, Journal of Nuclear Materials, Vol. 568, 153899, 2022.
[3] S. H. Baek, H.-S. Shim, J. G. Kim, and D. H. Hur, Effects of heat flux on fuel crud deposition and sub-cooled nucleate boiling in simulated PWR primary water at 13 MPa, Annals of Nuclear Energy, Vol. 133, pp. 178–185, 2019.
[4] R. Adamson, F. Garzarolli, B. Cox, A. Strasser, P. Rudling, Corrosion Mechanisms in Zirconium Alloys, A.N.T. International, 2007, Sweden.
[5] T. Kim, K. J. Choi, S. C. Yoo, Y. Lee, and J. H. Kim, Influence of dissolved hydrogen on the early stage corrosion behavior of zirconium alloys in simulated light water reactor coolant conditions, Corrosion Science, Vol. 131, pp. 235–244, 2018.
[6] M. P. Puls, The Effect of Hydrogen and Hydrides on the Integrity of Zirconium Alloy Components, Springer, London, 2012.